Research Article

3D high-content screening for the identification of compounds that target cells in dormant tumor spheroid regions

Carsten Wenzel[a], Björn Riefke[a], Stephan Gründemann[a], Alice Krebs[a], Sven Christian[a], Florian Prinz[a], Marc Osterland[a], Sven Golfier[a], Sebastian Räse[a], Nariman Ansari[b], Milan Esner[c], Marc Bickle[c], Francesco Pampaloni[b], Christian Mattheyer[b], Ernst H. Stelzer[b], Karsten Parczyk[a], Stefan Prechtl[a], Patrick Steigemann[a,*]

[a]Bayer Pharma AG, Global Drug Discovery, Muellerstrasse 178, 13353 Berlin, Germany
[b]Physical Biology Group, Buchmann Institute for Molecular Life Sciences (BMLS), Goethe University Frankfurt, Germany
[c]Max Planck Institute of Molecular Cell Biology and Genetics, High-Throughput Technology Development Studio (TDS), Dresden, Germany

ARTICLE INFORMATION

ABSTRACT

Cancer cells in poorly vascularized tumor regions need to adapt to an unfavorable metabolic microenvironment. As distance from supplying blood vessels increases, oxygen and nutrient concentrations decrease and cancer cells react by stopping cell cycle progression and becoming dormant. As cytostatic drugs mainly target proliferating cells, cancer cell dormancy is considered as a major resistance mechanism to this class of anti-cancer drugs. Therefore, substances that target cancer cells in poorly vascularized tumor regions have the potential to enhance cytostatic-based chemotherapy of solid tumors.

With three-dimensional growth conditions, multicellular tumor spheroids (MCTS) reproduce several parameters of the tumor microenvironment, including oxygen and nutrient gradients as well as the development of dormant tumor regions.

We here report the setup of a 3D cell culture compatible high-content screening system and the identification of nine substances from two commercially available drug libraries that specifically target cells in inner MCTS core regions, while cells in outer MCTS regions or in 2D cell culture remain unaffected. We elucidated the mode of action of the identified compounds as inhibitors of the respiratory chain and show that induction of cell death in inner MCTS core regions critically depends on extracellular glucose concentrations. Finally, combinational treatment with cytostatics showed increased induction of cell death in MCTS. The data presented here shows for the first time a high-content based screening setup on 3D tumor spheroids for the identification of substances that specifically induce cell death in inner tumor spheroid core

regions. This validates the approach to use 3D cell culture screening systems to identify substances that would not be detectable by 2D based screening in otherwise similar culture conditions.

Introduction

One of the main properties of cancer cells is sustained proliferative growth. Accordingly, the cell cycle is a major target for chemotherapy. Cytostatic drugs show strong anti-cancer efficacy in conventional *in vitro* assays; however, findings from 2D cell culture based experiments can only be partially translated to experimental outcomes *in vivo* and resistance to chemotherapy is still a frequent cause for treatment failure in patients with advanced and inoperable cancer. Several factors confer resistance to standard treatment regimens including, but not limited to, pharmacokinetic properties, genetic heterogeneity, drug clearance by cancer cells [1–4]. As commonly used cytostatics mainly target proliferating cells, tumor cell dormancy could be a factor for a limited response to these compounds [5,6].

Tumor cell dormancy is influenced by regional differences in oxygen and nutrient supply within the neoplastic tissue, depending on the amount and quality of (neo-) vascularization (*i.e.* the distance from supplying blood vessels). As tumor growth requires high amounts of energy and nutrients, tumor cell proliferation is therefore mainly restricted to regions adjacent to blood vessels and human tumor tissue can show relatively low proliferative indices in poorly perfused areas [3,5,7,8]. Cancer tissue can therefore be subdivided, depending on vascularization, into well-supplied, proliferating tumor cell regions in the vicinity of blood vessels and mostly dormant cells in poorly vascularized tumor regions.

Dormant cancer cells could potentially lead to disease relapse after cytostatic-based chemotherapy. Therefore, targeting this cell population could be of interest to enhance cytostatic-based chemotherapy [6].

Despite the potential role of dormant cells in limiting the effectiveness of cytostatic-based chemotherapy, few efforts have been made to specifically target this tumor cell population [6,9,10]. This could be due to the fact, at least in part, that there is a lack of appropriate screening-compatible *in vitro* models that are able to simulate the metabolic microenvironment in tumors.

Recently, 3D cancer cell culture models have gained interest, as they have the potential to mimic the complex three dimensional organization of tumor tissue *in vivo*. Similar to native tumor tissue, cells cultured as multicellular tumor spheroids (MCTS) show strong proliferation gradients that reflect distribution gradients of oxygen, nutrients and energy, as well as the accumulation of metabolites from outer to inner spheroid regions [3,4,11–13]. However, conventional 3D-based methods are not able to identify localized phenotypes in 3D models. Therefore we set up a high throughput, high-content microscopy compatible 3D MCTS assay on 384-well microtiter plates to identify substances that specifically target dormant cells in MCTS core regions. As a proof of principle, we screened two small compound libraries and identified nine hits that specifically target cells in inner tumor spheroid regions, while cells in outer regions or cultured under 2D cell culture conditions remain unaffected. We identified all hits as being inhibitors of the respiratory chain and further characterized their mode of action in MCTS. Finally, we showed additive effects in combination therapy with selected compounds when combined with cytostatics *in vitro*.

Materials and methods

Spheroid generation

Spheroid generation was carried out using a modified version of the liquid overlay cultivation technique described previously [14]. For the generation of imaging-compatible 3D tumor spheroids, 10 µl of a heated 1.5% w/v agarose (in DMEM without phenol red and fetal bovine serum (FBS)) solution was dispended by liquid dispensers (Multidrop Combi, Thermo Scientific) into sterile 384-well clear bottom imaging plates. To prevent premature gelation of the agarose suspension, the multidrop and dispensing cassette was heated by infrared lamps. For tumor spheroid seeding, a single cell suspension was seeded into agarose-coated (1.5% w/v) 384-well clear bottom plates in 40 µl RPMI1640 containing 10% (v/v) FBS supplemented with 1% Penicillin/Streptomycin (and 0.01 µg/ml insulin for T47D cells (Gibco)) using a liquid dispenser. Cell lines seeding number was optimized to obtain spheroids with an approximate diameter of 400 µm on day 4 and were seeded in following density: 2000 cells per well (c/w) for T47D, 5000 c/w for DLD1, 2000 c/w for DU145, and 1000 c/w for primary colon cancer cells. For schematic overview please see Supplementary Fig. S2.

The plates were incubated under standard cell culture conditions at 37 °C and 5% CO_2 in humidified incubators for 4 days to allow formation of reproducible spheroids of defined size and morphology. In general approximately 50% of all tested cell lines are capable of spheroid formation in these conditions. As described by others [15] spheroid formation can be facilitated by addition of low percentage of reconstituted basement membrane preparation if cells are not capable of forming compact spheroids (*e.g.*, BD Matrigel). Drugs (Enzo Life Sciences Screen-Well® FDA Approved Drug library (640 compounds) and Screen-Well® ICCB Known Bioactives library (480 compounds)) were added in 20 µl culture medium for additional 3 days.

Prior to imaging, spheroids were stained for 24 h by adding Hoechst 33342 (1 mg/ml, Life Technologies) as counterstain for all nuclei and Sytox Green, as stain for dead cells (2 mM, Life Technologies) at a final dilution of 1:10,000 each.

Image acquisition

One image per spheroid and wavelength, focused on the spheroid center was captured by Molecular Devices Micro widefield system with a 2 × objective. Quantification of inner core cell death was

done with MetaXpress software (Molecular Devices) using custom written image analysis routines. Briefly, spheroid borders were detected on Hoechst channel and masks were generated, scaled down and transferred on to the Sytox Green channel to quantify cell death in inner spheroid regions. All images were captured as 12-bit tiff files and no non-linear corrections have been applied.

3D image acquisition was done on a custom build mDSLM microscopy system as described earlier [16]. Briefly samples were dehydrated in an ascending ethanol series (50%, 70%, 85%, and 99%) for 5 min each. Then spheroids were transferred to benzyl alcohol/benzyl benzoate (1:1, v/v), transferred in a glass capillary and imaged using $2.5 \times$ illumination objective and $10 \times$ detection objective. 142 z-planes with 2.58 µm spacing were imaged for T47D spheroid in movie 1, 137 z-planes were imaged for anti-mycin A (100 nM) treated MCTS. 3D reconstruction and movie generation was done with Imaris software (Bitplane).

Cytotoxicity assay

For 2D toxicity assessment T47D cells were seeded at 2250 cells per well (c/w) in 40 µl on 384-well plates and were allowed to attach for 24 h. After 3 days drug incubation, cell viability was determined. Hoechst (1 mg/ml) and Sytox Green (2 mM) were used for staining at a final concentration of 1:10,000. Cell death index was calculated by counting all cells (as detected by Hoechst staining) divided by the number of Sytox Green positive dead cells.

Cell titer glo assay

Viability for *in vitro* combination studies in MCTS was measured with Cell Titer Glo Assay (Promega). To support reagent penetration, lysis and ATP recovery from MCTS an equal volume of reagent was added to sample and shaken for 15 min at 450 rpm. Luminescence readout was done after 30 min incubation at room temperature.

Immunohistochemistry

Prior to harvesting, spheroids were fixed for 24 h in 4% PFA. Then spheroids were transferred to 50 mL tubes (Falcon), washed twice in ice-cold DPBS and equilibrated in 30% sucrose (w/v) DPBS solution for 1 h. Then spheroids were transferred to cryomolds and covered in Tissue-Tek OCT compound. After 30 min of equilibration cryomolds were frozen by incubation in a mixture of dry ice and 2-methylbutane (Sigma Aldrich). Prepared samples were cut into 5 µm sections by cryostat, mounted on SuperFrost Plus slides (Menzel-Glaser) and then rehydrated in DPBS for 20 min. After 1 h in blocking and permeabilization solution (1% BSA, 0.1%Triton, 0.1% TWEEN-20) the primary antibody was incubated overnight at 4 °C. Incubation and staining with Hypoxyprobe-1 kit (Hypoxyprobe-1, Chemicon), mouse monoclonal IgG1 labeled with FITC and cell labeling with Click-iT EdU imaging kit (Alexa Fluor 555 azide, Life Technologies) were done according to the respective manufacturers instructions. After staining, slides were mounted in Slowfade Gold (Life Technologies) and imaged on AxioInvert 500 (Carl Zeiss) with $10 \times$ air objective and attached camera.

T47D breast cancer cell harvesting and NMR spectroscopy

For the extraction of metabolites and sample preparation for ^{1}H NMR spectroscopy the protocol from [17] was adapted to T47D breast cancer cells. In brief, cells were washed, methanol quenched and transferred for subsequent extraction. Spectra of extracted aqueous metabolite phase were acquired in 3 mm NMR tubes at 600.13 MHz and 300 K using a Bruker AVANCE III spectrometer equipped with a TCI-Cryo-Probe and a sample jet system (Bruker BioSpin). The residual water signal was suppressed by a 1D-NOESY presaturation pulse sequence. Typically, a total of 512 transients each of 64 k data points was acquired with an acquisition time of 2.65 s, an interpulse delay of 4 s, a spectral width of 20 ppm and a pulse width of 8.2 µs at 5 dB (90°). The free induction decay (FID) was multiplied by a 0.3 Hz exponential line-broadening factor to improve the signal-to-noise ratio prior to Fourier transformation. Phase correction and referencing were performed using Topspin 2.1 (Bruker BioSpin). For the baseline correction ACD Software Suite 12 (ACD/Labs) was used. The TSP signal was set to 0.00 ppm.

NMR data analysis

Multivariate analysis of the integrated bucket data was performed using SIMCA-P software (version 13.0, Umetrics AB) applying pareto scaling. Unsupervised principal components analysis (PCA) and supervised models (PLS-DA, OPLS-DA) were used to extract the main drivers, or spectral regions of the spectra responsible for group separation.

Metabolites were manually annotated and quantified with the help of the Chenomx NMR Suite 7.5 (Chenomx Inc.). The metabolite concentrations were expressed in (mM) using the integrated TSP region (0.025 mM). The heatmap was built using the same called function of GNU R 3.0.1. Data was logarithmized in advance and clustered with hierarchical clustering using Euclidean distance measure and complete linkage agglomeration.

Seahorse

Oxygen consumption rate (OCR) and extracellular acidification rate (ECAR) were measured with an XF^e Extracellular Flux Analyzer (Seahorse Bioscience) according to manufacturer's instructions. In brief, cells were plated at 25,000 cells/well on 96-well multiplates (Custom Seahorse cell culture plates) in standard cell culture medium. After 24 h media was exchanged to non-buffered RPMI1640 containing 11 mM glucose and 2 mM glutamine and equilibrated in a CO_2-free incubator for 1 h. XF assay consisted of sequential mix, pause and measurement steps, allowing determination of OCR and ECAR every 10 min for up to 180 min. The concentrations used in this assay are given in Supplementary Table 1.

Mesoscale AMPK activation

AMPK activation was determined by MSD (meso scale discovery) assay for human duplex (phospho) alpha1-AMPK on threonine 172. Samples were collected following manufacturer's instructions and adjusted to same protein concentrations (30 µg/well). Phosphorylated AMPK was normalized to total AMPK amount and used as readout for AMPK activation.

Quantitative reverse transcription PCR

RNA was extracted using the 6100 NucleicPrepStation (Applied Biosystems) according to manufacturer's instructions and quantified on the 8-channel Nanodrop spectrophotometer (ND-8000, Thermo Scientific). cDNA was produced using the GeneAmp® RNA PCR Kit (Life Technologies) and quantitative reverse transcription PCR (RT-qPCR) was conducted using Applied Biosystems TaqMan® Gene Expression Assays before analysis on the 7900 PCR machine (Applied Biosystems). Relative mRNA levels were calculated to the geometric mean of reference genes ACTB (encoding Beta-actin) and RPL13A (encoding 60S ribosomal protein L13a). Full gene names: ACYL (ATP citrate lyase), GLUT1 (solute carrier family 2 (facilitated glucose transporter), member 1), ANGPTL4 (angiopoietin-like 4), BNIP3 (BCL2/adenovirus E1B 19 kDa interacting protein 3), CA9 (carbonic anhydrase IX), VEGFA (vascular endothelial growth factor A).

Statistical analysis and hit evaluation

One-way ANOVA tests for combination therapy experiments were done using Prism software (GraphPad). Significance of differences between multiple groups was compared using a Bonferroni posttest analysis. RT-qPCR gene expression levels and AMPK activation levels were compared by multiple t-test using Prism software (two-tailed t-test with Welch's correction).

Normalization, quality control, hit list generation and fitting curves for AC_{50} determination of identified hit compounds were done with Genedata Screener® for high-content screening and Genedata Condoseo modules (Genedata AG).

Results

With three-dimensional growth conditions, multicellular tumor spheroids (MCTS) mimic several parameters of the tumor microenvironment *in vivo*. Based on their ability to effectively form compact MCTS from a single cell suspension within 4 days (Movie 1—formation of a T47D MCTS from a single cell suspension, Fig. 1A and Movie 2—illustration of a compact T47D MCTS after 4 days incubation), we chose the T47D human breast cancer cell line as an initial model system.

Supplementary material related to this article can be found online at http://dx.doi.org/10.1016/j.yexcr.2014.01.017.

Cells in inner MCTS core regions experience similar conditions as cancer cells in poorly vascularized tumor regions. In both situations, concentration gradients of oxygen and nutrients, as well as the accumulation of metabolites contribute to the formation of an unfavorable microenvironment. Indeed, MCTS slices stained with anti-pimonidazole antibody, a marker for hypoxia, showed strong hypoxia (<10 mmHg oxygen tension) deep inside the MCTS (Supplementary Fig. S1). Accordingly, as compared to the same cells cultured in 2D cell culture in otherwise identical culture conditions, T47D spheroids showed up-regulation of hypoxia- and low nutrition responsive genes (Fig. 1B).

Proliferation in tumor tissue occurs mainly in well-nourished regions adjacent to supplying blood vessels reflecting the need for high amounts of nutrients and energy for proliferation while cells in nutrient deprived and hypoxic tumor regions remain mostly dormant [3,6,7]. Similarly, proliferation in T47D spheroids can be detected mainly in outer MCTS layers, while inner MCTS core regions remain dormant (Fig. 1C).

As inner MCTS cells do not proliferate, we tested their response to cytostatic therapy. Thus, we incubated T47D MCTS for 3 days either with cisplatin or paclitaxel, two routinely used chemotherapeutic agents. Similar to their toxic effect in 2D cell culture (data not shown) these compounds induced widespread cell death in T47D MCTS after 3 days of incubation (Fig. 1D). However, cell death only occurred in outer spheroid regions, as a viable MCTS core could be isolated after recovery from cytostatic treatment and removal of the dead cell layer. In contrast, treatment with staurosporine, a general cytotoxic agent, led to complete dissolution of the tumor spheroid and widespread cell death (Fig. 1D and E). Therefore we conclude that dormant inner MCTS cells can resist cisplatin and paclitaxel therapy.

For the generation of high numbers of reproducible 384-well agarose-coated spheroid-containing plates for screening purposes, we adapted the setup reported by Friedrich et al. [14] for automated microscopy by using sterile clear bottom microtiter plates and heated automatic liquid dispensers (see Material and methods and Supplementary Fig. S2) for plate production.

This setup resulted in the generation of highly uniform and reproducible spheroids with one spheroid per well ($n=1536$ spheroids on four 384-well plates, standard deviation of total spheroid area $+/-7.5\%$).

To visualize spheroids and dead cells for high-content analysis, fluorescent dyes with sufficient penetration in MCTS were used. Images from the Hoechst 33342 channel were used to automatically identify the total spheroid area and generate a mask, which was then used as the region for intensity measurement in the Sytox Green channel (visualizing cell death). Cell death in total spheroids as well as in inner and outer spheroid regions was measured and hits were characterized by a higher ratio of cell death induced in inner tumor spheroid regions as compared to outer regions (see Fig. 2A). Using this setup with one image per wavelength taken at the center of the spheroid, we screened two commercially available drug libraries (Enzo Life Sciences Screen-Well FDA Approved Drug library (640 compounds) and Screen-Well ICCB Known Bioactives library (480 compounds)), which comprise a total of 1120 ($n=3$ replicas) compounds (for setup and high-content screening procedures, see Material and methods and Fig. 2A) in one week. Given an average imaging time of 20 min per plate on an automated imaging system and two runs per week this assay would be able to yield a minimum throughput of 40,000 compounds per week in a high-throughput setup.

With a threshold of >30% intensity of the staurosporine general cytotoxicity control (cell death measured by Sytox Green staining intensity, median of 3 replicas), 44 compounds could be identified that induce cell death in 3D tumor spheroids (black line parallel to the X-axis in Supplementary Fig. S3A). For the identification of compounds that specifically induce cell death in inner MCTS regions, we generated masks to measure Sytox Green intensity (cell death) in inner core and outer ring regions of the MCTS (see Fig. 2A for illustration) and calculated the ratio of the intensity in inner core region *versus* intensity in the outer layer. Compounds were characterized as hits if the intensity in the Sytox Green channel (cell death) was at least 5× stronger in inner core as compared to the outer MCTS region (see Fig. 2A for illustration and black line parallel to the Y-axis in Supplementary Fig. S3A). Nine hits that specifically led to cell death in inner MCTS
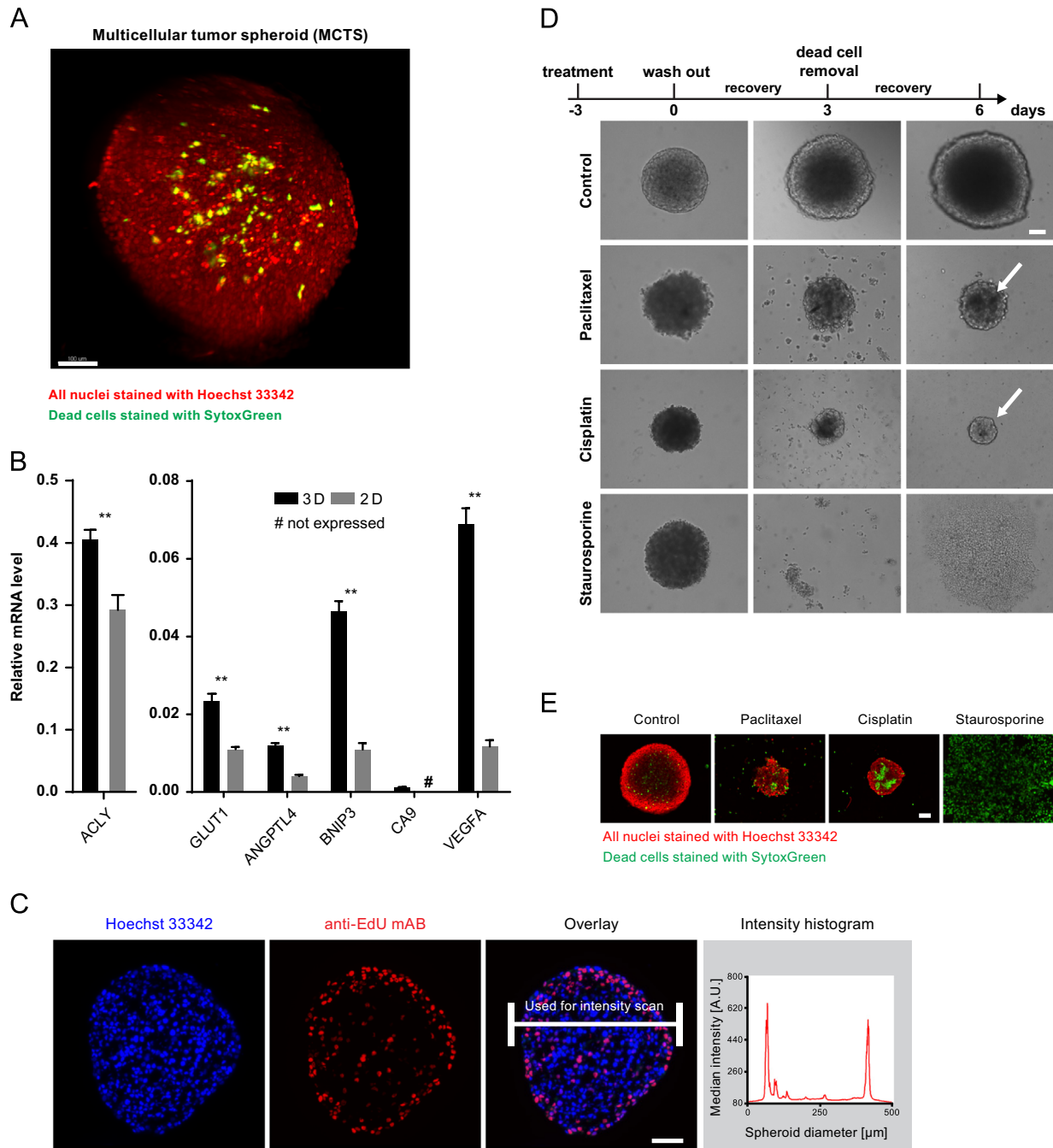
Fig. 1 – Multicellular tumor spheroids (MCTS) mimic several parameters of the tumor microenvironment. (A) T47D breast cancer MCTS: 2D projection of a 3D image stack of 142 *z*-planes with 2.58 μm spacing showing the organization of T47D spheroids. Cell nuclei are stained with Hoechst (red) and dead cells are labeled with Sytox green (green). Scale bar, 100 μm. Please see also Movie 1. **(B)** RT-qPCR shows up-regulation of hypoxia- and low nutrition responsive genes in MCTS compared to standard 2D cell culture conditions. Geometric mean of reference genes ACTB and RPLP13A were used for normalization of all RT-qPCR results. Bars show average of 3 biological replicates (+SD), **$p < 0.01$. For full gene names see material and methods. **(C)** Cryosections of an untreated spheroid cultured for 5 days, stained with Hoechst (blue) and incubated 18 h with EdU probe (red). EdU, as a thymidine analog, is incorporated into DNA in *S*-phase and indicates proliferating cells. Mainly outer cell layers of the MCTS show EdU incorporation (see histogram of EdU signal in MCTS cross section). Scale bar, 100 μm. **(D)** Cytostatics, paclitaxel (100 nM) and cisplatin (100 μM), mainly affect the outer proliferative layer in MCTS, which could be removed after 3 days treatment and 3 days of recovery by pipetting. An inner cytostatic-resistant viable core could be isolated (arrows). The staurosporine (10 μM) cytotoxic control leads to complete disruption of the MCTS. Scale bar, 100 μm. **(E)** Sytox green staining shows that isolated cytostatic-resistant cores (see D) are viable. Scale bar, 100 μm.
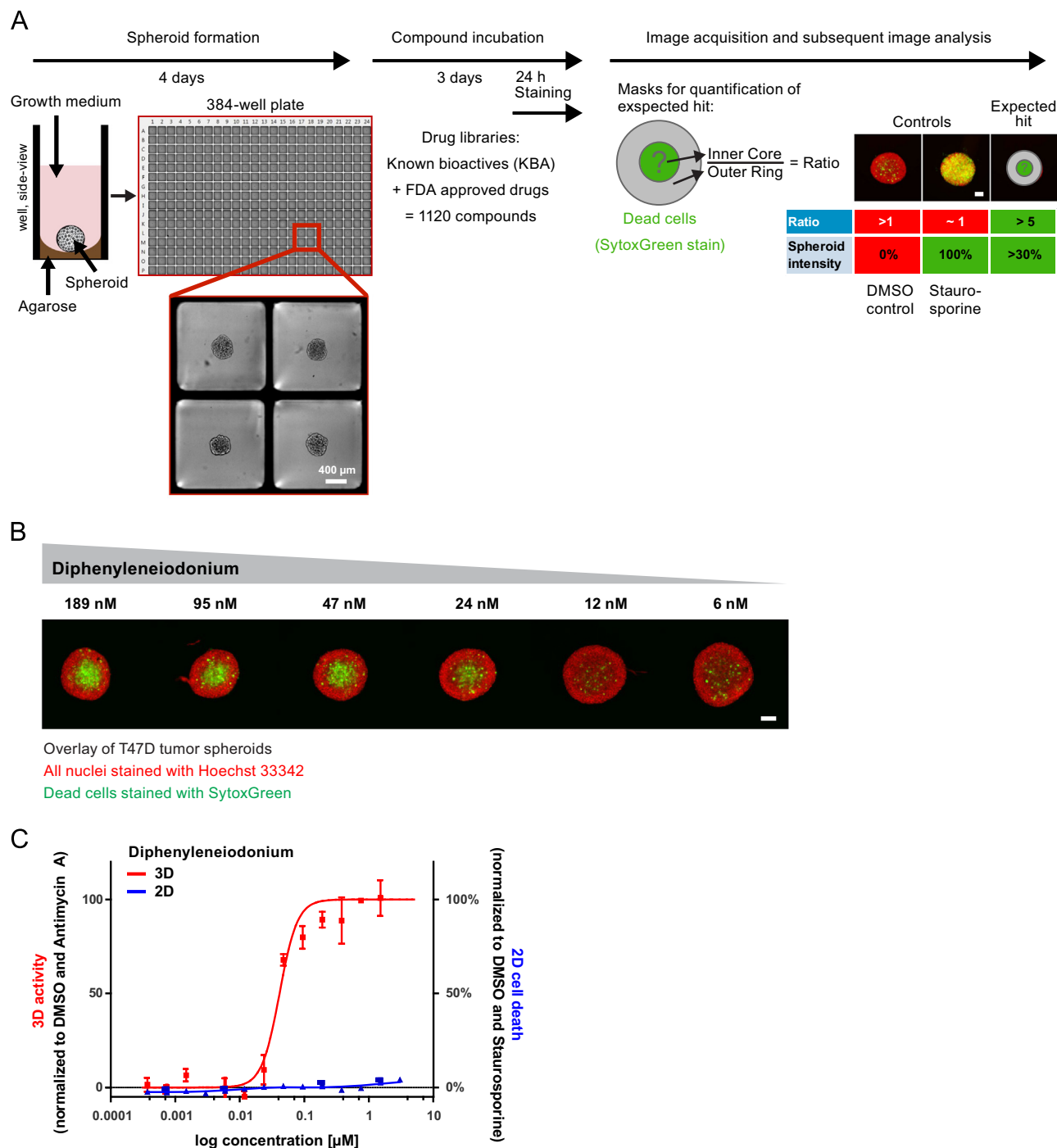
Fig. 2 – High-content screening (HCS) on multicellular tumor spheroids (MCTS). (A) HCS-workflow for T47D MCTS generated on 384-well agarose-coated multiplates. Development of custom image analysis routines allowed automated compound evaluation to specifically identify induction of cell death in MCTS core regions. Used drug libraries consisted of 1120 compounds with known bioactivity (KBA) and a set of FDA approved drugs. Staurosporine=general cytotoxicity control. Scale bar, 100 µm. (B) Representative images of a dilution series of the screening hit diphenyleneiodonium. Scale bar, 100 µm. (C) Comparison of dose response curve from screening hit diphenyleneiodonium on 3D spheroids vs. 2D cell culture. Similar results were obtained with all screening hits (see Supplementary Fig. S3C).

regions (while cells in the outer regions remained viable) could be identified (Fig. 2B and Fig. S4). The Hitlist is provided in Table 1 and a 3D reconstruction of a treated MCTS in Movie 3 shows that the MCTS inner core death phenotype can indeed specifically be observed in the inner MCTS core region, while the outer cell layer remains unstained. All of the nine identified compounds show a similar phenotype and did not induce cell death in 2D cell culture at similar culture conditions (Fig. 2C and Supplementary Fig. S3C).

Supplementary material related to this article can be found online at http://dx.doi.org/10.1016/j.yexcr.2014.01.017.

Table 1 – Identified hits that induce cell death in MCTS core regions and hit expansion with respiratory chain inhibitors with respective AC$_{50}$ (inner core death) values.

Compound name	Library	AC$_{50}$ (3D)	Proposed mode of action
Primary hits			
AG-879	**KBA**	20 μM	
Diphenyleindonium	**KBA**	62 nM	
MBCQ	**KBA**	8 μM	
Miconazole	**FDA**	22 μM	
Nefazodone	**FDA**	15 μM	
Oligomycin A	**KBA**	3 nM	Complex V inhibition
Pimozide	**FDA/KBA**	11 μM	
QNZ	**KBA**	1 nM	
Valinomycin	**KBA**	3 nM	Uncoupler
Hit expansion			
Antimycin A		20 nM	Complex III
Atpenin A5		<50 μM	Complex II
Berberine		17 μM	
Dinitrophenol		24 μM	Uncoupler
FCCP		6 μM	Uncoupler
Metformin		5 mM	
Pentamidine		30 μM	
Phenformin		142 μM	
Rotenone		7 nM	Complex I
Tyrphostin 9		1 μM	

For first categorization, we next studied if interactions between the identified hits exist. In a drug interaction matrix setup we tested whether the combination of two compounds would lead to an additive effect on MCTS compared to the single compounds. However, all different combination treatments showed similar phenotypes as the single compound treatment (Supplementary Fig. S4).

Two of the hit compounds, oligomycin A and valinomycin, are well-known inhibitors of the respiratory chain (Complex V inhibitor and ionophore, respectively [18]). Therefore we tested all hits for their effect on cellular respiration by direct measurement of alterations in oxygen consumption and lactate generation using electro-optical detection based XF^e extracellular flux analyzer on 2D cell cultures (see Material and methods). We found that all hits affected oxygen consumption or lactate production and therefore can be categorized as respiratory chain inhibitors (Fig. 3A and B).

Supporting this finding, all compounds altered the metabolic fingerprint of MCTS in a similar manner as measured by NMR based spectroscopy and cluster together with known respiratory chain inhibitors (see heatmap, Fig. 3C).

In a next step, we investigated the effect of compounds that are known to act specifically on certain components of the respiratory chain (Complex I, II, III, ATP synthase, see Table 1). All these compounds led to similar phenotypes with cell death induction in inner core regions of MCTS (Table 1 hit expansion and Supplementary Fig. S4) and show no or only weak effects in 2D cell culture (Supplementary Fig. S3C). Taken together, we conclude that all identified compounds affect cellular respiration and that inhibition of the respiratory chain leads to cell death specifically in core regions of MCTS.

Additionally, MCTS core death after respiratory chain inhibition could also be induced on MCTS from different cancer cell lines (e.g., colorectal adenocarcinoma DLD-1 cell line, epithelial prostate cancer cell line DU145) and spheroids generated from primary colon cancer biopsies (colon cancer liver metastasis-derived primary cell line) (Fig. 4A). These results show that oxidative phosphorylation is required for cell survival in dormant MCTS core regions of tumor spheroids derived from various tumor cell lines.

Inhibition of the respiratory chain leads to cellular energy stress which is sensed by AMP-activated protein kinase (AMPK). AMPK is activated by high AMP/ATP ratios and serves to reprogram the cellular metabolism to resist low energy conditions by enhancing catabolic pathways that generate ATP and reduction of ATP consuming processes [19,20].

Indeed, inhibiting the respiratory chain with different inhibitors (Antimycin A—Complex III, Metformin—Complex I, Rotenone—Complex I, Nefazodone) induced AMPK activation in MCTS (Fig. 4B). However, AMPK activation alone is not sufficient to induce cell death in inner tumor spheroid core regions as addition of AMPK activators AICAR, PT-1 or Salicylate did not result in MCTS core death (Supplementary Fig. S5A).

MCTS inner tumor spheroid cell death is preceded by caspase activation as visualized by caspase 3/7 sensitive live cell staining (see Movie 4 for caspase activation in inner core regions and also Movie 5 showing a time delayed onset of cell death after activation of caspases, quantification is provided in Fig. 4C). Additionally, the pan-caspase inhibitor Z-VAD-FMK leads to a partial rescue of the phenotype induced by blocking the respiratory chain (Fig. 4D).

Supplementary material related to this article can be found online at http://dx.doi.org/10.1016/j.yexcr.2014.01.017.

Taken together we conclude that inhibition of the respiratory chain leads to AMPK activation and to induction of apoptosis in MCTS core regions.

Two main energy producing pathways supply tumor cells with ATP: oxidative phosphorylation and glycolysis. Therefore, we speculated that outer MCTS cells (or cells cultured in 2D), with direct access to glucose from the surrounding medium, could switch to energy production by glycolysis and therefore prevent
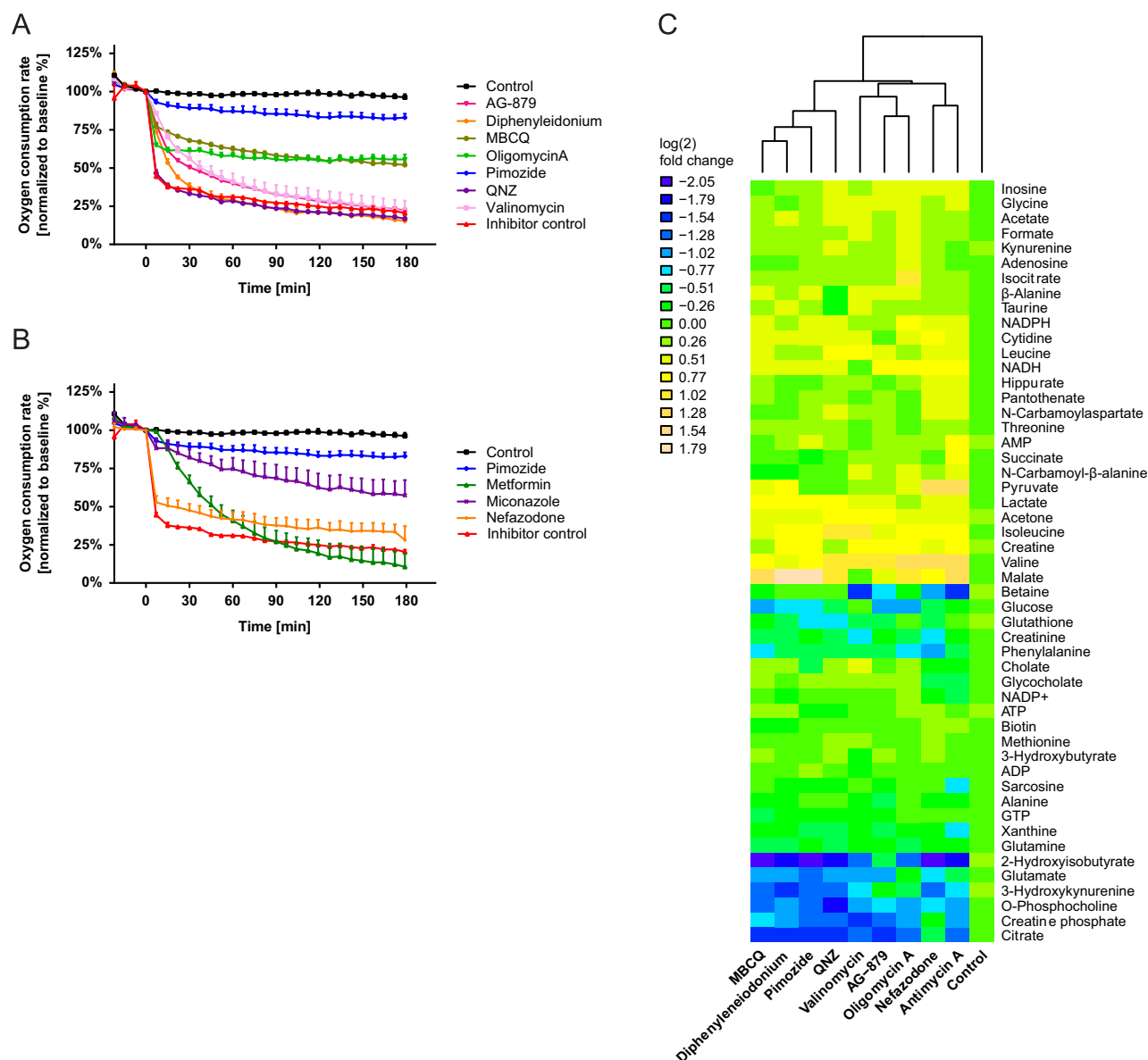
Fig. 3 – Identified compounds that induce cell death in MCTS core regions act as respiratory chain inhibitors. (A and B) Strong to moderate decrease of oxygen consumption rate of T47D cells incubated with denoted hit compounds (inhibitor control = complex I inhibitor rotenone, 1 μM). For concentrations used please see Supplementary Table S1. Graph shows average of 3 replicates. Error bars indicate +SEM. (C) Driver metabolites were measured by NMR spectroscopy and annotated, quantified and clustered with hierarchical clustering using Euclidean distance measure and complete linkage agglomeration. Heatmap clustering reveals close clustering of identified hits with known respiratory chain inhibitors (Valinomycin and oligomycin A). Scale, log(2) fold-change. For concentrations used please see Supplementary Table S1.

cell death while cells in inner MCTS regions with lower glucose levels [21] would experience stronger energy stress and become sensitive to the inhibition of the respiratory chain. Indeed, varying glucose levels in the surrounding media directly influenced the severity of the phenotype of respiratory chain inhibition. High glucose concentrations prevent cell death in inner MCTS core regions in response to inhibitors of the respiratory chain while lowering glucose levels broadened the region and intensity of cell death in MCTS (Fig. 5A), leading to cell death in the entire MCTS in glucose-free conditions. Accordingly, co-addition of cytochalasin B or 2-Deoxy-D-glucose (2-DG), inhibitors of cellular glucose uptake or glycolysis, respectively, also lead to cell death in the entire MCTS,

while solely inhibiting glucose transport or incubation in glucose-free media does not induce cell death in MCTS (Fig. 5B). Therefore, we conclude that the amount of available glucose in the extra-cellular environment is a major determinant for sensitivity of MCTS cells against inhibitors of the respiratory chain.

Respiratory chain inhibitors target dormant cells in poorly supplied dormant MCTS core regions. Therefore, a combination with cytostatics that additionally target the proliferative cell layer could have an additive effect on MCTS cell death. To target proliferating cells, we treated DLD1 and T47D tumor spheroids for 3 days with paclitaxel or cisplatin and subsequently added metformin or antimycin A for another 3 days to additionally target the dormant cell population in
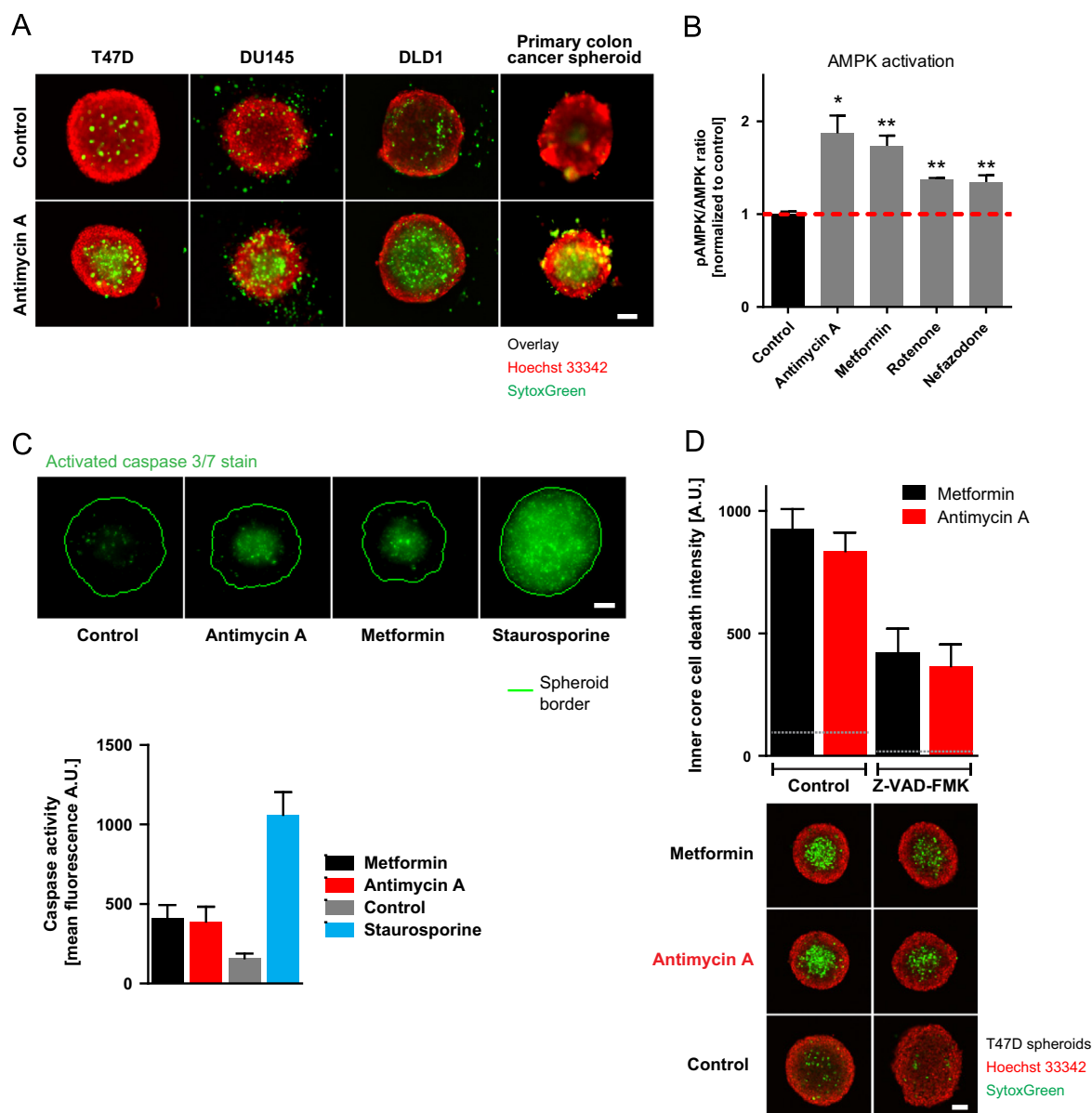
Fig. 4 – (A) Death in MCTS core regions after respiratory chain inhibition in different cancer cell lines. Antimycin A (100 nM) induces cell death in core regions in breast cancer cell line T47D, prostate cancer cell line DU145, colorectal cancer cell line DLD1, and primary spheroids. Scale bar, 100 µm. **(B)** Increased phosphorylation state of AMPK on threonine 172 as a marker for AMPK activation. Ratio of pAMPK to AMPK was increased in T47D spheroids after 24 h incubation with respiratory chain inhibitors (100 nM antimycin A, 10 mM metformin, 100 nM rotenone, 10 µM nefazodone+untreated DMSO control). $**p < 0.05$, $*p < 0.1$, two-tailed t-test with Welch's correction. Error bars indicate +SD, $n=2$. **(C)** Cell death in MCTS core regions is preceded by caspase 3/7 activation (green=CellEvent Caspase 3/7 stain). Staurosporine (10 µM) was used as positive control for caspase activation. Antimycin A and metformin were used at 100 nM and 10 mM (spheroids treated for 72 h), respectively. Please see also Movie 4 for a time-lapse visualization of caspase activation. Bars in the graph shows average of 4 replicates+SD. Scale bar in the image, 100 µm. **(D)** Inner core death in T47D spheroids (treated for 72 h) can be partially rescued by pan-caspase inhibition (Z-VAD-FMK, 100 µM). Error bars indicate +SD, $n=8$. Scale bars, 100 µm.

the MCTS core. Indeed, combination treatment had an additive effect on MCTS overall cell death (Figs. 6A and B).

Discussion

Cytostatic-based chemotherapy is a commonly used therapeutic regimen for cancer treatment. However, cytostatics mainly target proliferating cancer and are less effective against dormant cells which could be a possible cause for only partial remission and relapse of tumors after therapy [5,22,23]. Therefore, a therapeutic option to target dormant tumor regions could support cancer therapy.

3D multicellular tumor spheroids (MCTS) reproduce several parameters of tumors *in situ*. By integrating automated liquid handling systems for plate production, spheroid seeding,
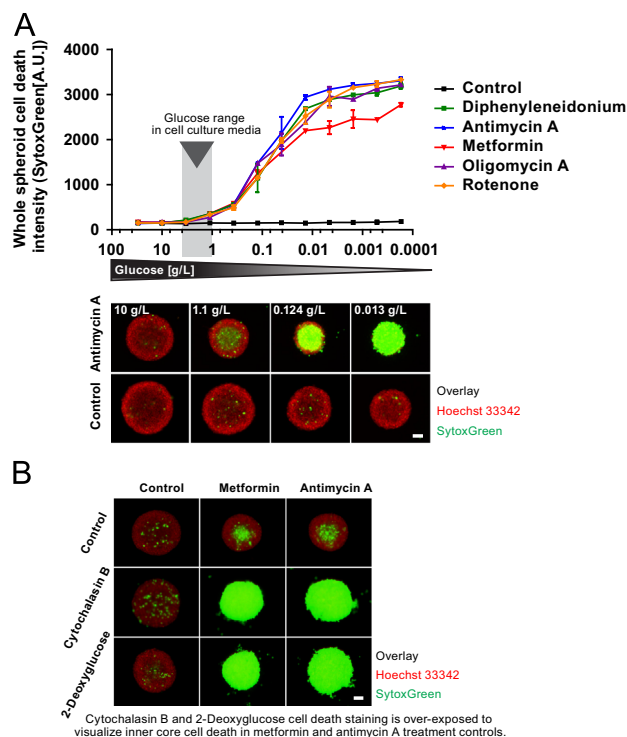
Fig. 5 – Glucose concentration in the extracellular environment is a major determinant for sensitivity of MCTS cells against inhibitors of the respiratory chain. (A) High glucose concentrations prevent cell death in inner tumor spheroid core regions in response respiratory chain inhibitors and conversely, low glucose levels lead to a strengthening of the phenotype. For concentrations used please see Supplementary Table S1. Plot shows average of Sytox Green staining intensity of 4 replicates+/−SD. (B) Co-addition of cytochalasin B (10 μM) or 2-Deoxy-D-Glucose (50 mM), an inhibitor of cellular glucose uptake or glycolysis respectively, lead to cell death in the entire spheroid while inhibition of glucose transport or inhibition with 2-DG alone has no effect (controls). Scale bars, 100 μm.

generation of homogenous spheroids with one spheroid per well and staining procedures, we here present a 384-well microtiter plate based workflow for high-throughput high-content based screening on 3D cell culture. High-content analysis allows assessment of cell death with spatial resolution and the identification of substances that specifically induce localized cell death inside the MCTS. As a proof of principle, we screened two commercially available compound libraries, and identified several substances that specifically lead to cell death in dormant MCTS regions.

Our results indicate that all identified compounds act by a similar mode of action and direct measurements of oxygen consumption show that all identified substances interfere with the proper function of the respiratory chain—either by acting as inhibitors or uncouplers of the respiratory chain. Interestingly, for induction of cell death in inner MCTS core regions the exact target in the respiratory chain seems to be irrelevant, as complex I inhibitors induce similar phenotypes as complex III/V inhibitors or uncouplers of the respiratory chain.

Given that cancer cells are predominantly glycolytic (Warburg effect) and the observation that the targeted cells are located in tumor areas with lower oxygen supply, the identification of respiratory chain inhibitors to selectively target cells in MCTS core regions was rather surprising. However, MCTS slices stained with pimonidazole, a marker for hypoxia, (Supplementary Fig. S1) shows that the targeted dormant cells are not hypoxic but rather are located in regions of intermediate oxygen supply, with anoxia only in the innermost spheroid regions. Accordingly, inhibitors of the respiratory chain had no additional effect when cultivated under hypoxic (1% O_2) conditions (data not shown). Similar distributions can also be observed in tumor models, in which proliferation occurs in the regions adjacent to the supplying blood vessels, followed by dormant intermediate oxygenated regions not yet stained positive for pimonidazole [3,6,7]. Therefore, we conclude that the identified compounds lead to cell death in regions of MCTS, in which respiration is still possible and required for cell survival.

Cells in MCTS core regions strongly depend on respiration for survival—possibly because of low levels of glucose that do not allow glycolysis to provide sufficient ATP. Accordingly, supplementation of high glucose concentrations in the medium rescues and lowering glucose levels strengthens the phenotype induced by inhibition of the respiratory chain. This and complete spheroid cell death after co-treatment with either an inhibitor of glucose uptake (Cytochalasin B) or glycolysis (2-Deoxyglucose) indicates that the level of glucose supply is one of the major determinants of sensitivity of dormant cells to respiratory chain inhibition.

As growth media supplements and culture conditions have the potential to strongly influence the phenotype and therefore screening outcome, these findings identifies media composition (*e.g.*, glucose concentration) and culture conditions (*e.g.*, oxygen levels) as important factors that may further need to be adjusted. Even though 3D tissue culture better reflects the situation in the tumor than 2D cell culture these models still remain artificial. Medium composition and culture conditions need to closely reflect the *in vivo*-situation to support the identification of hits with higher possibility to translate *in vitro* results to an effect *in vivo*.

Based on the observation that respiratory chain inhibitors induce cell death in dormant MCTS regions but do not affect the proliferative layer, we expected weak efficiency in single therapy and additive effects when combined with cytostatics that additionally target the proliferative layer. The results presented here show increased induction of cell death in MCTS when respiratory chain inhibitors are combined with cytostatics *in vitro* (Fig. 6A). In summary, our data suggest that targeting cytostatic-resistant tumor cells in dormant tumor regions with respiratory chain inhibitors could be a therapeutic option that could enhance the effectiveness of cytostatic-based chemotherapy.

However, a major question regarding these results is, if the mechanisms identified here can be translated into anti-tumor activity *in vivo*. Indeed, several complex I inhibitors show anti-tumor activity *in vivo*, especially in combination with cytostatics [24–26]. *In vitro* the effect induced by inhibitors of the respiratory chain is dependent on extracellular levels of glucose. Interestingly, metformin is in use as an anti-diabetic drug. Therefore the reported cancer-protective effect [27] of metformin could be induced by a combination of both, inhibition of complex I and additionally lowering blood glucose levels.
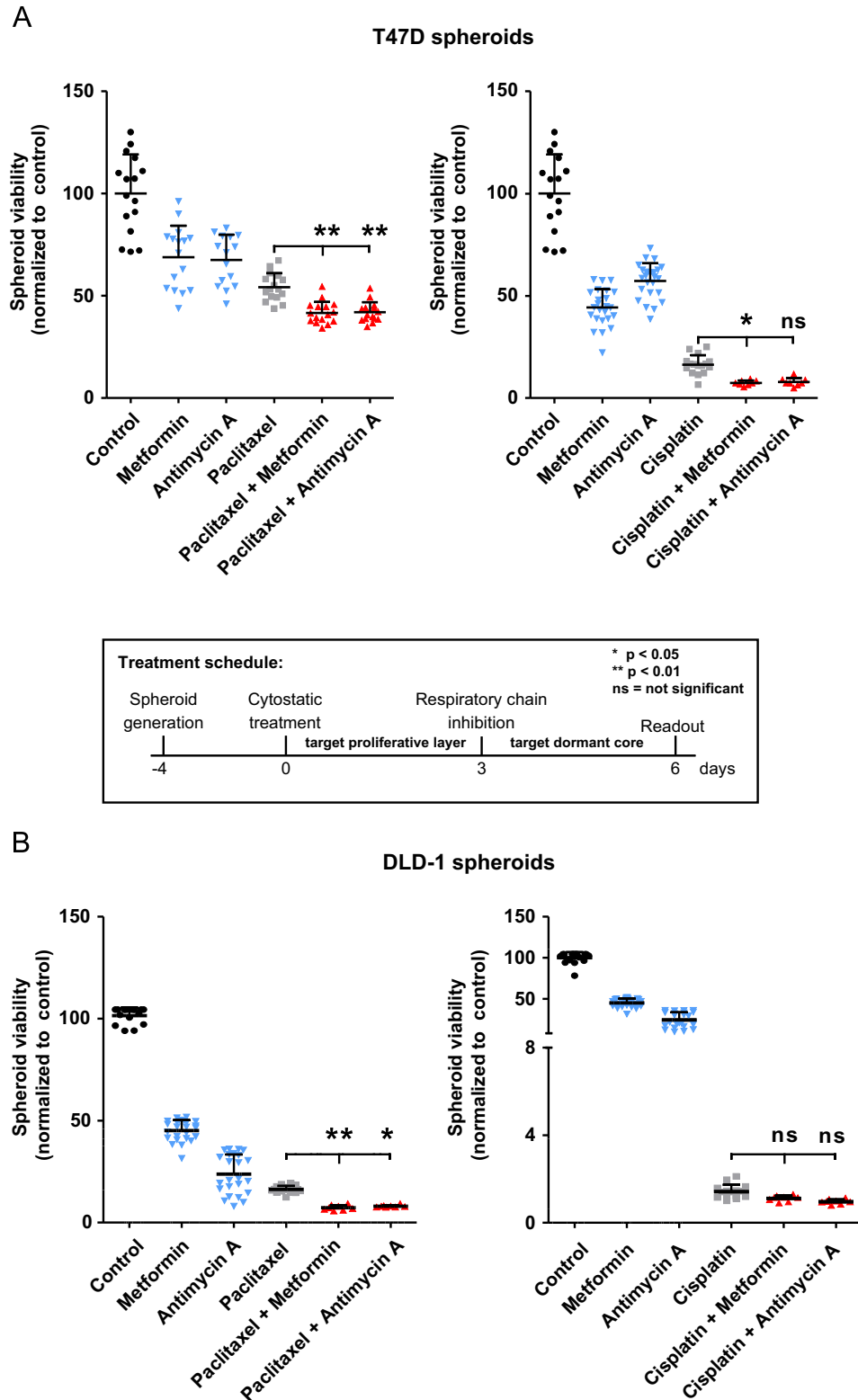
Fig. 6 – Combination therapy with cytostatics increases efficiency of respiratory chain inhibitors. (A) *In vitro* combination therapy on T47D breast cancer spheroids. Combination of paclitaxel (100 nM) or cisplatin (100 μM) with either metformin (10 mM) or antimycin A (100 nM) significantly increases overall cell death in MCTS model. Bar shows average of >16 replica+SD. (B) *In vitro* combination therapy on DLD1 colorectal adenocarcinoma spheroids shows increased induction of overall cell death in the MCTS model. Bar shows average of >16 replicates+SD.

Given that oxidative phosphorylation is the main energy source for most eukaryotic cells, inhibition of the respiratory chain is considered to be rather toxic on the whole organism level. However, we identified FDA approved compounds which are used in the clinic but act as respiratory chain inhibitors (*e.g.*, miconazole, pimozide, metformin). Interestingly, these compounds show either only mild effect on cellular respiration (limited effectiveness in reducing oxygen consumption in the seahorse assay) (pimozide, miconazole) or slow kinetics (metformin) but induce a similar phenotype in MCTS as more effective inhibitors (Supplementary Fig. S5B).

Thus, already partial inhibition of the respiratory chain could be sufficient for anti-cancer activity *in vitro*.

Conclusion

In conclusion we show here that 3D high-content screening enables the identification of compounds that specifically target cells in inner tumor spheroid core regions and that would not be identified in 2D based screening approaches in otherwise similar culture conditions. We show that a class of hits that induce cell death specifically in inner tumor spheroid core regions consist of inhibitors of the respiratory chain and that their phenotype critically depends on extracellular glucose concentrations. These findings could facilitate the establishment of secondary assays in more extensive screening campaigns for early hit classification and identification of non-respiratory chain hit classes with similar phenotypes in the hit list. Furthermore we show that media composition and culture conditions influence the phenotype and should be carefully considered while setting up a 3D tumor spheroid-based screening campaign.

Conflict of interests

Acknowledgments

Appendix A. Supplementary materials

Supplementary data associated with this article can be found in the online version at http://dx.doi.org/10.1016/j.yexcr.2014.01.017.

REFERENCES

[1] M. Dean, T. Fojo, S. Bates, Tumour stem cells and drug resistance, Nat. Rev. Cancer 5 (2005) 275–284.

[2] A. Marusyk, V. Almendro, K. Polyak, Intra-tumour heterogeneity: a looking glass for cancer? 12 (2012) 323–334Nat. Rev. Cancer 12 (2012) 323–334.

[3] A.I. Minchinton, I.F. Tannock, Drug penetration in solid tumours, Nat. Rev. Cancer 6 (2006) 583–592.

[4] O. Trédan, C.M. Galmarini, K. Patel, I.F. Tannock, Drug resistance and the solid tumor microenvironment, J. Natl. Cancer Inst. 99 (2007) 1441–1454.

[5] J.A. Aguirre-Ghiso, Models, mechanisms and clinical evidence for cancer dormancy, Nat. Rev. Cancer 7 (2007) 834–846.

[6] A.H. Kyle, J.H.E. Baker, A.I. Minchinton, Targeting quiescent tumor cells via oxygen and IGF-I supplementation, Cancer Res. 72 (2012) 801–809.

[7] L. Huxham, A. Kyle, J. Baker, Microregional effects of gemcitabine in HCT-116 xenografts, Cancer Res. 64 (2004) 6537–6541.

[8] R.P. Sullivan, G. Mortimer, I.O. Muircheartaigh, Cell proliferation in breast tumours: analysis of histological parameters Ki67 and PCNA expression, Ir. J. Med. Sci. 162 (1993) 343–347.

[9] S. Awale, J. Lu, S.K. Kalauni, Y. Kurashima, Y. Tezuka, S. Kadota, et al., Identification of arctigenin as an antitumor agent having the ability to eliminate the tolerance of cancer cells to nutrient starvation, Cancer Res. 66 (2006) 1751–1757.

[10] J. Lu, S. Kunimoto, Y. Yamazaki, Kigamicin D, a novel anticancer agent based on a new anti-austerity strategy targeting cancer cell's tolerance to nutrient starvation, Cancer Sci. 95 (2004) 547–552.

[11] F. Hirschhaeuser, H. Menne, C. Dittfeld, J. West, W. Mueller-Klieser, L.A. Kunz-Schughart, Multicellular tumor spheroids: an underestimated tool is catching up again, J. Biotechnol. 148 (2010) 3–15.

[12] R.R. Sutherland, Cell and environment interactions in tumor microregions: the multicell spheroid model, Science 240 (1988) 177–184.

[13] K. LaRue, M. Khalil, J. Freyer, Microenvironmental regulation of proliferation in multicellular spheroids is mediated through differential expression of cyclin-dependent kinase inhibitors, Cancer Res. 64 (2004) 1621–1631.

[14] J. Friedrich, C. Seidel, R. Ebner, L.A. Kunz-Schughart, Spheroid-based drug screen: considerations and practical approach, Nat. Protoc. 4 (2009) 309–324.

[15] A. Ivascu, M. Kubbies, Rapid generation of single-tumor spheroids for high-throughput cell function and toxicity analysis, J. Biomol. Screen. 11 (2006) 922–932.

[16] P.J. Verveer, J. Swoger, F. Pampaloni, K. Greger, M. Marcello, E.H.K. Stelzer, High-resolution three-dimensional imaging of large specimens with light sheet-based microscopy, Nat. Methods 4 (2007) 311–313.

[17] Athersuch TJT Ellis JKJJK, R. Cavill, R. Radford, C. Slattery, P. Jennings, et al., Metabolic response to low-level toxicant exposure in a novel renal tubule epithelial cell system, Mol. Biosyst. 7 (2011) 247–257.

[18] D.G. Nicholls, S.L. Budd, Mitochondria and neuronal survival, Physiol. Rev. 80 (2000) 315–360.

[19] B. Faubert, G. Boily, S. Izreig, T. Griss, B. Samborska, Z. Dong, et al., AMPK is a negative regulator of the warburg effect and suppresses tumor growth in vivo, Cell Metab. 17 (2012) 113–124.

[20] G.R. Steinberg, B.E. Kemp, AMPK in Health and Disease, Physiol. Rev. 89 (2009) 1025–1078.

[21] J.J. Casciari, S.V. Sotirchos, R.M. Sutherland, Glucose diffusivity in multicellular tumor spheroids glucose diffusivity in multicellular tumor spheroids, Cancer Res. 48 (1988) 3905–3909.

[22] D. Páez, M.J. Labonte, P. Bohanes, W. Zhang, L. Benhanim, Y. Ning, et al., Cancer dormancy: a model of early dissemination and late cancer recurrence, Clin. Cancer Res. 18 (2012) 645–653.

[23] S.A. Menchón, C.A. Condat, Quiescent cells: a natural way to resist chemotherapy, Phys. A: Stat. Mech. Appl. 390 (2011) 3354–3361.

[24] F. Vazquez, J.-H. Lim, H. Chim, K. Bhalla, G. Girnun, K. Pierce, et al., , PGC1α expression defines a subset of human melanoma tumors with increased mitochondrial capacity and resistance to oxidative stress 23 (2013) 287–301Cancer Cell 23 (2013) 287–301.

[25] R. Haq, J. Shoag, P. Andreu-Perez, S. Yokoyama, H. Edelman, G.C. Rowe, et al., Oncogenic BRAF regulates oxidative metabolism via PGC1α and MITF, Cancer Cell (2013) 302–315.

[26] I. Ben Sahra, J.-F. Tanti, F. Bost, The combination of metformin and 2 deoxyglucose inhibits autophagy and induces AMPK-dependent apoptosis in prostate cancer cells, Autophagy (2010) 6.

[27] J.M.M. Evans, L.A. Donnelly, A.M. Emslie-Smith, D.R. Alessi, A.D. Morris, Metformin and reduced risk of cancer in diabetic patients, Br. Med. J. 330 (2005) 1304–1305.